

1451 **Chapter 5**
1452 **Relativistic Cyclotron**

1453 **Abstract** This chapter introduces to the AVF (azimuthally varying field), isochronous,
1454 relativistic cyclotron, and to the theoretical material needed for the simulation exer-
1455 cises. A brief reminder of the historical context is followed by further basic theoretical
1456 considerations leaning on the cyclotron concepts introduced in Chapter 4 and in-
1457 cluding

- 1458 - Thomas focusing and the AVF cyclotron,
- 1459 - positive focusing index,
- 1460 - isochronous optics,
- 1461 - separated sector cyclotrons,
- 1462 - spin dynamics in an AVF cyclotron.

1463 Simulation exercises use optical elements and keywords met earlier: the analytical
1464 field modeling DIPOLE, TOSCA in case using a field map is preferred, CAVITE to
1465 accelerate, SPNTRK to solve spin motion, FAISCEAU, FAISTORE, FIT, etc. The
1466 exercises further develop on radial and spiral sector magnets, edge focusing and
1467 flutter, isochronous optics, separated sector ring cyclotrons, and their modeling as
1468 part of DIPOLE, DIPOLES and other CYCLOTRON keyword capabilities.

1469 **Notations used in the Text**

$B; B_0$	field value; at reference radius R_0
$\mathbf{B}; B_R; B_\theta; B_y$	field vector; radial, azimuthal and axial components
$B\rho = p/q; B\rho_0$	ion rigidity; reference rigidity
$C; C_0$	orbit length, $C = 2\pi R$; reference, $C_0 = 2\pi R_0$
E	ion energy
EFB	effective Field Boundary
\mathcal{F}, F	azimuthal field form factor; flutter, $F = \left(\frac{\langle (\mathcal{F} - \langle \mathcal{F} \rangle)^2 \rangle}{\langle \mathcal{F} \rangle^2} \right)^{1/2}$
$f_{\text{rev}}, f_{\text{rf}}$	revolution and accelerating voltage frequencies
h	harmonic number, an integer, $h = f_{\text{rf}}/f_{\text{rev}}$
$k = \frac{R}{B} \frac{dB}{dR}$	geometric index, a global quantity
$n = \frac{\rho}{B} \frac{dB}{d\rho}$	focusing index, a local quantity
$m; m_0; M$	mass; rest mass; in units of MeV/c^2
$\mathbf{p}; p_0$	ion momentum vector; reference momentum
q	ion charge
R, R_0, R_E	average orbital radius, $R = C/2\pi$; $R(p = p_0)$; $R(E)$
\mathcal{R}	radial field form factor
1470 RF	Radio-Frequency: as per the accelerating voltage technology
s	path variable
$T_{\text{rev}}, T_{\text{rf}}$	revolution and accelerating voltage periods
v	ion velocity
$V(t); \hat{V}$	oscillating voltage; its peak value
x, x', y, y'	radial and axial coordinates in moving frame [$(*)' = d(*)/ds$]
α	momentum compaction, or trajectory deviation
$\beta = v/c; \beta_0; \beta_s$	normalized ion velocity; reference; synchronous
$\gamma = E/m_0$	Lorentz relativistic factor
$\Delta p, \delta p$	momentum offset
ε	wedge angle
ε_R	strength of a depolarizing resonance
ε_u	Courant-Snyder invariant (u stands for the coordinate: x, y, l, ...)
ζ	spiral angle of a spiral sector dipole EFB
θ	azimuthal angle
$\phi; \phi_s$	phase of oscillating voltage; synchronous phase

1471 **5.1 Introduction**

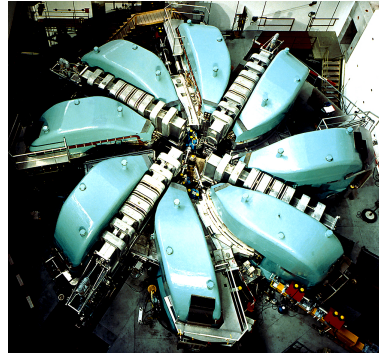
1472 Isochronous cyclotrons are in operation today by the thousands, tens are produced
1473 each year, applications include production of radio-isotopes mostly; proton therapy
1474 (Fig. 5.1), a rapidly growing field; high power beams and secondary particle beam

1475 production (Fig. 5.2). Cryogeny and high fields further allow compactness (Fig. 5.1)
 1476 as well as highest rigidity (Fig. 5.3)

Fig. 5.1 COMET proton-therapy cyclotron at PSI. A 250 MeV, 500 nA, 4-sector isochronous AVF cyclotron, the spiral poles enhance axial focusing. A 3 m diameter superconducting coil provides the dipole field [1]



Fig. 5.2 PSI 590 MeV ring cyclotron delivers a 1.4 MW proton beam. Acceleration takes ~ 180 turns; extraction efficiency is $> 99.99\%$; overall diameter is 15 m. Beam is used for the production of secondary neutron and muon beams [2]



1477 At the origin of the evolution towards the AVF cyclotron in the late 1930s is
 1478 the energy limitation, at a few 10s of MeV, of the classical cyclotron technology
 1479 (Chap. 4). Axial focusing in the latter is obtained by a slow decrease of the guiding
 1480 field with radius: a negative index $-1 < k < 0$, resulting in both radial and axial
 1481 periodic stability (Eq. 4.15). Isochronism requires instead the field to increase with
 1482 radius, field index $k > 0$, a consequence of $B(R) \propto \gamma(R)$ (Sect. 5.2). The AVF concept
 1483 by L.H. Thomas in 1938¹ [5] (Fig. 5.4), solved the problem: AVF results in periodic
 1484 stability as long as the field modulation parameter $F > \beta\gamma$ (Sect. 5.2.1). Spiral
 1485 pole geometry was introduced in 1954 [7] for increased axial focusing, allowing
 1486 greater k and isochronous acceleration to higher energy (Sect. 5.2.2). AVF cyclotrons

¹ The very L.H. Thomas of the eight years earlier Nature article on spin precession [6].

Fig. 5.3 RIKEN K2500, superconducting coil, separated-sector ring cyclotron [3]. The dipole field is 3.8 T, rigidity 8 Tm, diameter 18.4 m, 8,300 ton. Beam injection radius is 3.56 m, extraction radius is 5.36 m. The cyclotron is part of a heavy-ion accelerator complex [4]

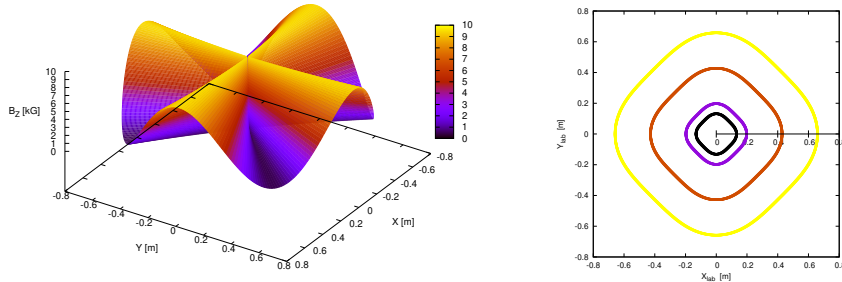
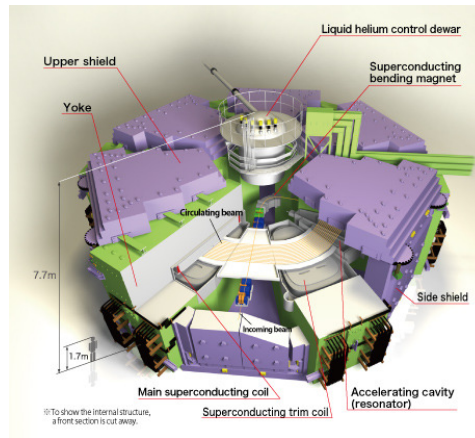


Fig. 5.4 A 4-periodic AVF cyclotron design (after Ref. [5]). Left: mid-plane azimuthally modulated field. Right: closed orbits around the cyclotron feature azimuthally varying curvature, greater on the hills, weaker in the field valleys

1487 were constructed to accelerate all sorts of ions, including polarized beams from
 1488 the moment polarized ion sources were available [8], whereas classical cyclotrons
 1489 gave up the land (Fig. 4.4). Applications included material science, radiobiology,
 1490 production of secondary beams. The separated sector method was developed in the
 1491 early 1960s, instances are today's high power PSI 590 MeV spiral sector cyclotron
 1492 (Fig. 5.2), brought into operation in 1974, and its injector-II, a radial-sector design
 1493 (Fig. 5.5). Iron-free regions between separated sector dipoles allowed room for
 1494 multiple high-Q RF resonators thus greater turn separation at extraction; for higher
 1495 efficiency extraction systems and thus higher beam current; and for the insertion of
 1496 beam instrumentation. Cyclotron energy subsequently increased, up to the present
 1497 days GeV range. Cryogeny was introduced in the early 1960s at the Michigan State
 1498 University K500 superconducting coil cyclotron [9] ($K = E A/Q^2$ is a measure of the
 1499 equivalent proton energy, 500 MeV in this case), allowing higher field and reduction
 1500 of size, culminating today with RIKEN's K2500 SRC (Fig. 5.3).

Fig. 5.5 PSI injector II, four separated radial sectors, 0.87 MeV injection energy, accelerates protons to 72 MeV in 100 turns. The drifts house 50.7 MHz RF systems and a flattop cavity. Injection is from the top, in the central region



Table 5.1 A comparison between an AVF and a separated sector cyclotron of same energy, 72 MeV, namely, the former AVF injector and the present Injector II of PSI high power cyclotron, after Ref. [8, p. 126])

		AVF	separated sector
Injection energy	keV	14	870
Extraction energy	MeV	72	72
Beam current	mA	0.2	1.6
Magnet		single dipole	4 sectors
Weight	ton	470	4 × 180
Gap	mm	240 to 450	35
$\langle B \rangle$; B_{\max}	T	1.6; 2	0.36; 1.1
RF system		180° dees	2 resonators
Max accelerating voltage	kV	2 × 70	4 × 250
RF frequency	MHz	50	50
Normalized beam emittance, hor.; vert.	μm	2.4; 1.2	1.2; 1.2
Beam phase width	deg	16 - 40	12
Energy spread	%	0.3	0.2
Turn separation at extraction	mm	3	18

1501 5.2 Basic Concepts and Formulae

1502 Mass increase with energy causes loss of synchronism in the classical cyclotron,
 1503 and the required negative field index (decreasing guiding field with radius) for
 1504 axial periodic motion stability adds to the effect. Isochronism instead, *i.e.*, constant
 1505 $\omega_{\text{rev}} = qB/\gamma m_0$, given orbit radius $R = \beta c/\omega_{\text{rev}}$, leads to positive index

$$k = \frac{R}{B} \frac{\partial B}{\partial R} = \frac{\beta}{\gamma} \frac{\partial \gamma}{\partial \beta} = \beta^2 \gamma^2 \quad (5.1)$$

1506 requiring k to follow the energy increase: the weak focusing condition $-1 < k < 0$
 1507 can not be satisfied, transverse periodic stability is lost.

1508 Isochronism requires the revolution period $T_{\text{rev}} = 2\pi\gamma m_0/qB$ to be momentum
 1509 independent; under this condition, differentiating this expression yields the radial

1510 field dependence

$$B(R) = \frac{B_0}{\gamma_0} \gamma(R) \quad (5.2)$$

1511 with B_0 and γ_0 some reference conditions,

1512 This led H.A. Bethe and M.E. Rose to conclude, in 1938, "... it seems useless
1513 to build cyclotrons of larger proportions than the existing ones... an accelerating
1514 chamber of 37 cm radius will suffice to produce deuterons of 11 MeV energy which
1515 is the highest possible..." [10]. "If you went to graduate school in the 1940s, this
1516 inequality [$-1 < k < 0$] was the end of the discussion of accelerator theory." (Frank
1517 Cole [11]).

1518 5.2.1 Thomas Focusing

1519 Whereas the classical cyclotron approach assumed revolution symmetry of the field,
1520 a 1938 publication stated: "[...] a variation of the magnetic field with angle, [...] of
1521 order of magnitude v/c ; together with nearly the radial increase of relative amount
1522 $\frac{1}{2}v^2/c^2$ of Bethe and Rose; gives stable orbits that are in resonance and not defo-
1523 cused." [5]. In other words, AVF in proper amount (Fig. 5.4) compensates the axial
1524 defocusing resulting from the increase of the field with radius (Eq. 5.2). Azimuthal
1525 field modulation and radial increase may be obtained by shaping the magnet poles,
as illustrated in Fig. 5.6.

Fig. 5.6 Pole shaping in an AVF cyclotron, an electron model, here [12]. The focusing pattern is FfFfFf, an alternation of strong (hill regions) and weak (valleys) radial focusing [13]



1526

1527 *Azimuthal field modulation, flutter*

1528 A simple approach to the $2\pi/N$ -periodic axial symmetry and field modulation may
1529 assume a sinusoidal azimuthal form factor

$$\mathcal{F}(\theta) = 1 + f \sin(N\theta) \quad (5.3)$$

1530 As an example, this is the case in Fig. 5.4. The mid-plane field can thus be expressed
1531 under the form

$$B(R, \theta) = B_0 \mathcal{R}(R) \mathcal{F}(\theta) \quad (5.4)$$

1532 with $\mathcal{R}(R)$ the radial dependence of the field. The orbit curvature varies along
1533 the $\frac{2\pi}{N}$ -periodic orbit, this requires distinguishing between the local focusing index
1534 $n = \frac{\rho(s)}{B(s)} \frac{dB}{d\rho}$ and the geometrical index k (Eq. 5.1), a global quantity which determines
1535 the wave numbers (Eq. 5.6). A “flutter” factor can be introduced to quantify the
1536 focusing effect of the azimuthal modulation,

$$F = \left(\frac{\langle (\mathcal{F} - \langle \mathcal{F} \rangle)^2 \rangle}{\langle \mathcal{F} \rangle^2} \right)^{1/2} \xrightarrow{\text{hard edge}} \left(\frac{R}{\rho} - 1 \right)^{1/2} \quad (5.5)$$

1537 wherein $\langle * \rangle = \oint (*) d\theta / 2\pi$. If the scalloping of the orbit (*i.e.*, its excursion in the
1538 vicinity of R) is of small amplitude, then $R \approx \rho$ and, accounting for the isochronism
1539 condition (Eq. 5.1), an approximate value of the wave numbers writes

$$\nu_R \approx \sqrt{1+k} = \gamma, \quad \nu_y \approx \sqrt{-k+F^2} \stackrel{\text{isochr.}}{=} \sqrt{-\beta^2 \gamma^2 + F^2} \quad (5.6)$$

1540 with the property

$$\nu_R^2 + \nu_y^2 = 1 + F^2 \xrightarrow{\text{hard edge}} \frac{R}{\rho} \quad (5.7)$$

1541 The flutter allows designing $-k + F^2 > 0$ (whereas $k > 0$), so ensuring vertical peri-
1542 odic stability. In the hypothesis of a sinusoidal azimuthal field modulation (Eq. 5.3)
1543 one has $F = f/\sqrt{2}$ and

$$\nu_y \approx \sqrt{-k + f^2/2}, \quad \nu_R^2 + \nu_y^2 = 1 + f^2/2 \quad (5.8)$$

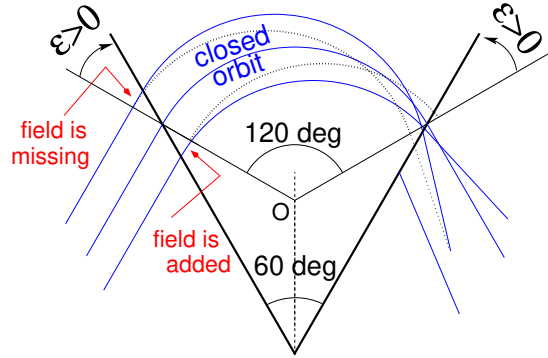
1544 *AVF Modeling*

1545 A numerical approach to the azimuthal modulation beyond the simple sine modula-
1546 tion of Eq. 5.3, is discussed in Sect. 18.2.6 (Eqs. 18.14, 18.18). It provides a modeling
1547 of $\mathcal{F}(\theta)$ over the whole beam excursion area, possibly including an R-dependence,
1548 $\mathcal{F}(R, \theta)$. The method ensures the continuity of $\mathcal{F}(R, \theta)$ and its derivatives, between
1549 neighboring magnetic sectors. The method is addressed further in the simulation
1550 exercises, where it is resorted to.

1551 *Wedge Focusing*

1552 In the entrance and exit regions of a bending sector, closed orbits are at an angle
 1553 to the iso-field lines, this causes “wedge focusing”, an effect sketched in Fig. 5.7:
 1554 with positive wedge angle ε , case of the AVF configuration, radial focusing decreases
 1555 whereas the angle of off mid-plane particle velocity vector to the azimuthal
 1556 component of the field in the wedge region causes axial focusing.

Fig. 5.7 A 120 deg bending of the closed orbit (curvature center at O) is ensured by a 60 deg bending sector. This results in a wedge angle ($\varepsilon > 0$ by convention in this configuration) in the transition regions between valleys and hills, which causes a decrease of the radial focusing (solid incoming trajectories, compared to dotted ones), and axial focusing under the effect of the trajectory angle to the azimuthal field component



1557 5.2.2 Spiral Sector

1558 Spiral sector geometry was introduced in 1954 in the context of FFA studies [7], and
 1559 found application in cyclotrons (as in PSI’s COMET cyclotron, Fig. 5.1). Spiraling
 1560 the edges (Fig. 5.8) results in stronger axial focusing (Eq. 5.11) compared to a
 1561 radial sector (Eq. 5.6), it also permits an increase of the wedge angle with radius, so
 1562 maintaining proper compensation of the increase of $k(R)$ (Eq. 5.1). In a spiral sector
 1563 bend the wedge angle is positive on one side of the sector, negative on the other
 1564 side (Fig. 5.8), with a global vertical focusing resultant. In a similar approach to the
 1565 periodic field modulation in a radial sector (Eq. 5.3), a convenient approach to the
 1566 spiral sector AVF uses

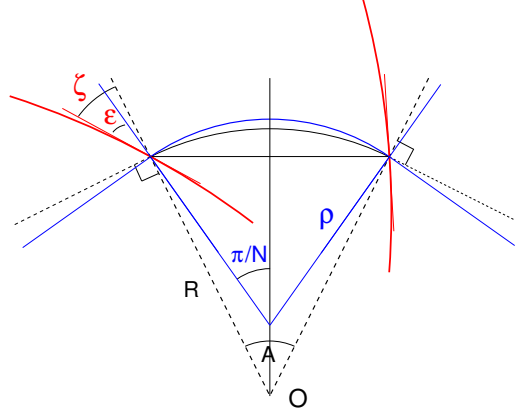
$$\mathcal{F}(R, \theta) = 1 + f \sin \left[N \left(\theta - \tan(\zeta(R)) \ln \frac{R}{R_0} \right) \right] \quad (5.9)$$

1567 with the spiral angle $\zeta(R)$ an increasing function of radius R , whereas the mid-plane
 1568 field is written under the form

$$B(R, \theta) = B_0 \mathcal{R}(R) \mathcal{F}(R, \theta) \quad (5.10)$$

1569 The local magnet edge geometry at R satisfies $r = r_0 \exp(\theta/\tan(\zeta))$, a logarithmic
 1570 spiral centered at the center of the ring, with ζ the angle between the tangent to the

Fig. 5.8 Geometrical parameters of a spiral sector dipole. The center of the ring is at O, ζ is the spiral angle (increasing with radius), ε is the wedge angle. In the hard edge field model, a line of constant field inside the sector is an arc of radius R ; thus the curvature radius ρ varies along the closed orbit in the dipole



1571 spiral edge and the ring radius (Fig. 5.8). This results in a larger contribution of the
1572 flutter term in the axial wave number,

$$v_y = \sqrt{-k + F^2(1 + 2 \tan^2 \zeta)} \quad (5.11)$$

1573 As the field index k increases with R to ensure isochronism (Eq. 5.1), the spiral angle
1574 follows so to maintain $-k + F^2(1 + 2 \tan^2 \zeta) > 0$. A limitation here is the maximum
1575 spiral angle achievable, obviously $\zeta \rightarrow 90$ deg.

1576 As an illustration, in TRIUMF cyclotron ζ reaches 72 deg in the 500 MeV region
1577 (from zero in the 100 MeV region) whereas $1 + 2 \tan^2 \zeta$ increases to 20 (from 1 in
1578 the 100 MeV region) and compensates a low $F < 0.07$ (down from $F = 0.3$). In PSI
1579 590 MeV cyclotron ζ reaches 35° on the outer radius. Most isochronous cyclotrons
1580 of a few tens of MeV use spiral sectors to benefit from the more efficient axial
1581 focusing [13].

1582 More can be found in the scaling FFAG chapter (Sect. 11.2.2) regarding the spiral
1583 sector, and regarding its numerical simulation.

1584 5.2.3 Isochronism

1585 In the hypothesis of isochronism, the revolution angular frequency satisfies $\omega_{\text{rev}} =$
1586 $c\beta(\gamma)/R(\gamma) = \text{constant}$. An orbital radius $R_\infty = c/\omega_{\text{rev}}$ is reached asymptotically as
1587 $\beta = v/c = R/R_\infty \rightarrow 1$. In terms of the RF frequency and harmonic number,

$$R_\infty = h \frac{c}{\omega_{\text{rf}}} \quad (5.12)$$

1588 Given $BR_\infty = \gamma m_0 c/q$ and using $\gamma = (1 - (R/R_\infty)^2)^{-1/2}$, the radial dependence of
1589 the field can be expressed in terms of R_∞ , namely,

$$B_0 \mathcal{R}(R) = \gamma B_0 = \frac{B_0}{\sqrt{1 - (R/R_\infty)^2}} \quad \text{with } B_0 = \frac{m_0 \omega_{\text{rev}}}{q} = \frac{m_0}{q} \frac{\omega_{\text{rf}}}{h} \quad (5.13)$$

1590 and goes to infinity with $R \rightarrow R_\infty$. For protons for instance, with $m_0/q = 1.6726 \times$
 1591 $10^{-27}[\text{kg}] / 1.6021 \times 10^{-19}[\text{C}] \approx 10^{-8}$, $BR_\infty[\text{T m}] = \gamma m_0 c / q \approx 3\gamma$. A typical value
 1592 for R_∞ can be obtained assuming for instance an upper $\gamma = 1.64$ (600 MeV) in a
 1593 region of upper field value $B = 1.64$ T, yielding $R_\infty \approx 3$ m.

1594 *Radial field law*

1595 From Eq. 5.13 it results that the radial field form factor of Eqs. 5.4, 5.10 can be
 1596 written

$$\mathcal{R}(R) = \left(1 - \left(\frac{R}{R_\infty}\right)^2\right)^{-1/2} \quad (5.14)$$

1597 A possible approach consists in using the Taylor expansion of $\mathcal{R}(R)$ (within the limits
 1598 of radius of convergence of that series), namely

$$\mathcal{R}(R) = 1 + \frac{1}{2} \left(\frac{R}{R_\infty}\right)^2 + \frac{3}{8} \left(\frac{R}{R_\infty}\right)^4 + \frac{5}{16} \left(\frac{R}{R_\infty}\right)^6 + \dots \quad (5.15)$$

1599 The coefficients in this polynomial in R/R_∞ are the field index and its derivatives,
 1600 they can be a starting point for further refinement of the isochronism, including for
 1601 instance side effects of the azimuthal field form factor $\mathcal{F}(R, \theta)$ (Eqs. 5.3, 5.9).

1602 The radial field index $k(R)$ in the AVF cyclotron is designed to satisfy the condition
 1603 of isochronism (Eq. 5.1). However, reducing the RF phase slip over the acceleration
 1604 cycle substantially below $\pm\pi/2$ requires a tolerance below 10^{-5} on field value over
 1605 the orbit excursion area. This tight constraint requires pole machining, shimming,
 1606 and other correction coil strategies in order to satisfy Eq. 5.1.

1607 *Fast Acceleration*

1608 Fixed field and fixed RF frequency allow fast acceleration, the main limitation is in
 1609 the amount of voltage which can be implemented around the ring. The voltage per
 1610 turn reaches 4 MV for instance at the PSI 590 MeV ring cyclotron, where bunches
 1611 are accelerated from 72 MeV to 590 MeV in less than 200 turns.

1612 Harmful resonances may have to be crossed as wave numbers vary during acceler-
 1613 ation, including the ‘‘Walkinshaw resonance’’ $\nu_R = 2\nu_y$ as $\nu_R \approx \gamma$ whereas the axial
 1614 wave number takes its value in the $\nu_y \approx 1^- \sim 1.5$ region. This coupling resonance
 1615 may result in an increase of vertical beam size and subsequent particle losses, fast
 1616 crossing mitigates the effect.

1617 Fast acceleration improves extraction efficiency, as the turn separation dR/dn is
 1618 proportional to the energy gain per turn (Sect. 5.2.4).

1619 5.2.4 Cyclotron Extraction

1620 The minimum radial distance between the last two turns, where the extraction septum
 1621 is located, is imposed by beam loss tolerances, which in some cases (high power
 1622 beams for instance) may be very tight, in the 10^{-4} range or less. Space charge in
 1623 particular matters, as it increases the energy spread, and thus the radial extent of
 1624 a bunch. In the relativistic cyclotron the separation between two consecutive turns
 1625 satisfies

$$\Delta R \approx \frac{\gamma}{\gamma + 1} \frac{\Delta E}{E} \frac{R}{v_R^2} \quad (5.16)$$

1626 with ΔE the effective acceleration rate per turn. Referring to Eq. 5.12, it indicates
 1627 that a greater RF harmonic allows greater extraction radius and benefits extraction
 1628 efficiency; it results from Eq. 5.16 that a large ring is an additional option for greater
 1629 turn separation at extraction, and as a matter of fact size is a limitation to intensity
 1630 in small cyclotrons.

1631 In low energy cyclotrons (γ close to 1), extraction efficiency may also be increased
 1632 by moving the wave number $\nu_R \approx \gamma$ close to the integer resonance $\nu_R = 1$.

1633 5.2.5 Resonant Spin Motion

1634 In the quasi-uniform, quasi vertical field $\mathbf{B} \approx \mathbf{B}_y$ of a classical cyclotron dipole, spins
 1635 quietly perform $G\gamma$ precessions around a vector $\omega_{sp} \parallel \mathbf{B}$ (Eq. 4.27) as the particle
 1636 velocity completes a 2π precession around the ring (Sect. 4.2.5).

1637 More is liable to happen in the AVF cyclotron, due to the strong radial field index
 1638 (Eq. 5.1) and to the azimuthal field modulation (Eqs. 5.3, 5.9): the azimuthal and
 1639 radial field components B_θ and B_R are non-zero out of the median plane, $\mathbf{B}(R, \theta, y)$
 1640 may locally depart from the vertical in a substantial manner, and so will the local pre-
 1641 cession vector $\omega_{sp}(R, \theta, y)$. The latter varies periodically in addition, as the particle
 1642 undergoes a vertical periodic motion about the median plane. Resonance between
 1643 spin precession (characterized by spin tune $\nu_{sp} = G\gamma$, Eq. 4.30) and periodic perturb-
 1644 ing field components (characterized by the vertical wave number ν_y , Eqs. 5.6, 5.11)
 1645 occurs if the two motions feature coinciding frequencies. This condition can be
 1646 expressed under the form

$$\nu_{sp} \pm \nu_y = \text{integer} \quad \text{or, equivalently} \quad G\gamma = \text{integer} \pm \nu_y \quad (5.17)$$

1647 The spin precession axis ω_{sp} moves away from the vertical as the spin motion gets
 1648 closer to resonance (during acceleration as $G\gamma$ varies for instance), to end up in the
 1649 median plane on the resonance.

1650 Consider now an ion bunch, away from any depolarizing resonance. Its polariza-
 1651 tion is $\langle S_y \rangle$, the average of the projection of the spins on the vertical. If a depolarizing
 1652 resonance is crossed during acceleration, the initial polarization (far upstream of the
 1653 resonance; index i) and final polarization (far downstream of the resonance; index f)

1654 satisfy the Froissart-Stora law [15],

$$\frac{\langle S_y \rangle_f}{\langle S_y \rangle_i} = 2e^{-\frac{\pi |\epsilon_R|^2}{2a}} - 1 \quad (5.18)$$

1655 wherein $|\epsilon_R|$ is the strength of the resonance: a measure of the strength of the
 1656 depolarizing fields, its calculation is addressed in a next chapter; a is the resonance
 1657 crossing speed,

$$a = G \frac{d\gamma}{d\theta} \pm \frac{dv_y}{d\theta} \quad (5.19)$$

1658 The Froissart-Stora formula indicates that, if the resonance is crossed slowly ($a \rightarrow$
 1659 0), $\langle S_y \rangle_f / \langle S_y \rangle_i \rightarrow -1$: spins follow the flipping motion of the precession axis,
 1660 polarization is flipped and preserved. If the crossing is fast ($a \rightarrow \infty$), $\langle S_y \rangle_f / \langle S_y \rangle_i \rightarrow$
 1661 0 , polarization is unaffected. Intermediate crossing speeds cause polarization loss:
 1662 $|\langle S_y \rangle|$ ends up smaller after the resonance.

1663 **5.3 Exercises**

1664 Exercises 5.2 to 5.4 use a field map, designed in exercise 5.1, to simulate an AVF
 1665 cyclotron dipole. Note that they can be performed using DIPOLE[S] analytical field
 1666 model instead, as in exercise 5.5 (a similar simulation which can be referred to is
 1667 exercise 4.2, Classical Cyclotron Chapter). As a reminder, regarding the interest of
 1668 one or the other of the two methods: field maps allow close to real field models
 1669 (a measured field map for instance, or from a magnet computer code); using an
 1670 analytical field model allows more flexibility regarding magnet parameters, which
 1671 can for instance be optimized using a matching procedure.

1672 **5.1 Modeling Thomas AVF Cyclotron**

1673 Solution: page 312.

1674 In this exercise a 2D mid-plane field map is built, inspired from Thomas's 1938
 1675 article [5]. The method to build the map is that of Exercise 4.1, TOSCA keyword
 1676 is used to raytrace through and derive the optical parameters of the 4-period AVF
 1677 cyclotron.

1678 (a) Construct a 360° 2D map of the median plane field $B_Z(R, \theta)$, simulating the
 1679 field in the 4-period Thomas cyclotron of Fig. 5.4, assuming the following:

1680 - $B_Z(R, \theta) = B_0[1 + f \sin(4(\theta - \theta_i))]$ (Eq. 5.3), with θ_i some arbitrary origin of
 1681 the azimuthal angle, to be determined. Hint: depending on θ_i value, the closed orbit
 1682 may be at an angle to the polar radius, as seen in Fig. 5.4; in that case TOSCA would
 1683 require non-zero in and out positioning angles TE and TS, to be determined and
 1684 stated using KPOS option [16]; instead, a proper choice of θ_i value allows a simpler
 1685 TE=TS=0;

1686 - an average axial field $B_0 = 0.5$ T on the 200 keV radius (the latter, $R_0(B_0)$, is to
 1687 be determined), $B_Z > 0$ and $0 < f < 1$ modulation.

1688 - an arbitrary field index k - a good idea is to start building and testing the AVF
 1689 in the case $k = 0$;

1690 - a uniform map mesh in a polar coordinate system (R, θ) as sketched in Fig. 4.17,
 1691 covering $R=1$ to 100 cm; take a radial increment of the mesh $\Delta R = 0.5$ cm, azimuthal
 1692 increment $\Delta\theta = 0.5 \text{ cm}/R_M$, with R_M some reference radius, say $R_M = 50$ cm, half
 1693 way between map boundaries;

1694 - an appropriate 6-column formatting of the field map data for TOSCA to read,
 1695 as follows:

1696 $R \cos \theta, Z, R \sin \theta, BY, BZ, BX$

1697 with θ varying first, R varying second in that list. Z is the vertical direction (normal
 1698 to the map mesh), so $Z \equiv 0$ in this 2D mesh.

1699 Provide a graph of $B_Z(R, \theta)$ over the extent of the field map.

1700 (b) Raytrace a few concentric closed trajectories centered on the center of the
 1701 dipole, ranging in $10 \leq R \leq 80$ cm. Provide a graph of these concentric trajectories
 1702 in the $(O; X, Y)$ laboratory frame, and a graph of the field along trajectories. Initial
 1703 coordinates can be defined using OBJET, particle coordinates along trajectories
 1704 during the stepwise raytracing can be logged in zgoubi.plt by setting IL=2 under
 1705 TOSCA.

- 1706 (c) Check the effect of the integration step size on the accuracy of the trajectory
 1707 and time-of-flight computation, by considering some Δs values in $[0.1, 10]$ cm, and
 1708 energies in a range from 200 keV to a few tens of MeV (considering protons).
 1709 (d) Produce a graph of the energy or radius dependence of wave numbers.
 1710 (e) Calculate the numerical value of the axial wave number, ν_y , from the flutter
 1711 (Eqs. 5.5, 5.6). Comparing with the numerical values, discrepancy is found: repeat
 1712 (d) for $f=0.1, 0.2, 0.3, 0.6$, check the evolution of this discrepancy.

1713 5.2 Designing an Isochronous AVF Cyclotron

1714 Solution: page 321.

- 1715 (a) Introduce a radius dependent field index $k(R)$ in the AVF cyclotron designed
 1716 in exercise 5.1, proper to ensure R-independent revolution period, in three different
 1717 cases of modulation: $f=0$ (no modulation), $f=0.2$ and $f=0.9$.

1718 Check this property by computing the revolution period T_{rev} as a function of
 1719 kinetic energy E_k , or radius R . On a common graph, display both T_{rev} and $dT_{\text{rev}}/T_{\text{rev}}$
 1720 as a function of radius, including for comparison a fourth case: $B=\text{constant}=5$ kG.

- 1721 (b) Provide a graph of the energy dependence of wave numbers.

1722 5.3 Acceleration to 200 MeV in an AVF Cyclotron

1723 Solution: page 327.

1724 In this exercise protons are accelerated to over 100 MeV in an AVF cyclotron:
 1725 well beyond the about 20 MeV energy reached in the classical cyclotron (see exer-
 1726 cise 4.10).

- 1727 (a) Produce an acceleration cycle of a proton, from 0.2 to 100 MeV, in the AVF
 1728 cyclotron designed in exercise 5.2. Note that a dedicated field map has to be created
 1729 in order to allow for the higher maximum energy - a 3 meter field map outer radius
 1730 works. Assume proper modulation coefficient f for axial focusing all the way to
 1731 300 MeV. Assume a double-dee design, and 400 keV peak voltage in the gap, use
 1732 CAVITE[IOPT=7] for acceleration to account for RF phase.

- 1733 (b) Give a graph of the energy dependence of wave numbers over the acceleration
 1734 range.

1735 5.4 Thomas-BMT Spin Precession in Thomas Cyclotron

1736 Solution: page 330.

1737 This exercise uses the field maps and input data file of exercise 5.3. Dependence
 1738 of energy boost on RF phase is removed by using CAVITE[IOPT=3] [16]. Consider
 1739 helion ions: use PARTICUL[Name=HELIUM] to define mass, charge and G factor,
 1740 all quantities needed for the integration of Thomas-BMT differential equation
 1741 (Eq. 4.27).

- 1742 (a) By scanning the vertical wave number, find the $G\gamma$ value for which the spin
 1743 motion resonance condition (Eq. 5.17) is satisfied.

- 1744 (b) Consider a particle with non-zero axial motion, so that it experiences hor-
 1745 izontal magnetic field components as it cycles around. Track its spin through the
 1746 resonance, take initial spin vertical $\mathbf{S} \equiv S_Z$. Provide a graph of S_Z as a function of
 1747 $G\gamma$ or energy.

1748 (c) Simulate resonance crossings for a series of different vertical motion ampli-
1749 tudes Z_0 ; produce a graph of these resonance crossings $S_Z(\text{turn})$.

1750 Plot the ratio $S_{y,f}/S_{y,i}(Z_0)$. From a match of this $S_{y,f}/S_{y,i}$ series with Eq. 5.18,
1751 show that the resonance strength changes in proportion to the vertical excursion.

1752 (d) Repeat (c) for a series of different resonance crossing speeds instead (Eq. 5.19),
1753 leaving Z_0 unchanged.

1754 Show that this $S_{y,f}/S_{y,i}$ series can be matched with Eq. 5.18.

1755 5.5 Isochronism and Edge Focusing in a Separated Sector Cyclotron

1756 Solution: page 334.

1757 This exercise uses DIPOLE to simulate a 30 deg sector dipole of a 4-period cy-
1758 clotron, and allow playing with field fall-off extent at dipole EFBs. The configuration
1759 of the cyclotron is typically that of PSI 72 MeV injector (Fig. 5.5). DIPOLE allows
1760 radial field indices up to the third order ($\partial^3 B_Z/\partial R^3$) [16, Eq. 6.3.18]. In question (b)
1761 however, higher order indices are needed to improve the isochronism, requiring the
1762 use of DIPOLES [16, Eqs. 6.3.20, 21].

1763 Take fringe fields into account (see Sect. 18.2.6), with

1764 - $\lambda = 7$ cm the fringe extent (changing λ changes the flutter, Eq. 5.5),

1765 - $C_0 = 0.1455$, $C_1 = 2.2670$, $C_2 = -0.6395$, $C_3 = 1.1558$ and $C_4 = C_5 = 0$, for a
1766 realistic field fall-off model.

1767 (a) Assume $k = 0$, here. Produce a model of a period using DIPOLE.

1768 Produce a graph of closed orbits across a period for a few different rigidities (FIT
1769 can be used to find them), and a graph of the field along these orbits.

1770 (b) In this question, R-dependence of the mid-plane magnetic field proper to
1771 ensuring energy independent revolution period is introduced. Use DIPOLES here,
1772 as it allows b_i field indices to higher order, as necessary to reach tight isochronism
1773 over the full energy range.

1774 Assume a peak field value $B_0 = 1.1$ T at a radius of 3.5 m in the dipoles. Find the
1775 average orbit radius R, and average field B (such that $BR = p/q$), at an energy of
1776 72 MeV.

1777 Determine a series of index values, $b_{i=1,n}$, in the model [16, Eq. 6.3.19]

$$B_Z(R, \theta) = B_0 \mathcal{F}(R, \theta) \left(1 + b_1 \frac{R - R_0}{R_0} + b_2 \left(\frac{R - R_0}{R_0} \right)^2 + \dots \right) \quad (5.20)$$

1778 proper to bring the revolution period closest to R-independent, in the energy range
1779 0.9 to 72 MeV (hint: use a Taylor development of Eq. 5.14 and identify with the
1780 R-dependent factors in Eq. 5.20).

1781 (c) Play with the value of λ , concurrently to maintaining isochronism with appro-
1782 priate b_i values. Check the evolution of radial and axial focusing - OBJET[KOBJ=5]
1783 and MATRIX can be used to get the wave numbers.

1784 From raytracing trials, observe that (i) the effect of λ on radial focusing is weak (a
1785 second order effect in the particle coordinates); (ii) greater (smaller) λ value results
1786 in smaller (greater) flutter and weaker (stronger) axial focusing (a first order effect).
1787 Note: the integration step size in DIPOLE[S] has to be consistent with the value

1788 field fall-off extent (λ value), in order to ensure that the numerical integration is
 1789 converged.

1790 (d) For some reasonable value of λ (normally, about the height of a magnet
 1791 gap, say, a few centimeters), compute $F^2 = \left\langle \left(\frac{B(\theta) - \langle B \rangle}{\langle B \rangle} \right)^2 \right\rangle$. Check the validity of
 1792 $v_y = -\beta^2 \gamma^2 + F^2$ (Eq. 5.6). MATRIX can be used to compute v_y , or multiturn
 1793 raytracing and a Fourier analysis.

1794 (e) Check the rule $F^2 \xrightarrow{\text{hard edge}} \frac{R}{\rho} - 1$ (Eq. 5.5), from the field $B(\theta)$ delivered by
 1795 DIPOLES. Give a theoretical demonstration of that rule.

1796 **5.6 A Model of PSI Ring Cyclotron Using CYCLOTRON**

1797 Solution: page 337.

1798 The simulation input data file in Tab. 5.2 is based on the use of CYCLOTRON, to
 1799 simulate a period of the eight-sector PSI ring cyclotron and work on the isochronism.
 1800 That file is the starting point of the present exercise.

1801 (a) With zgoubi users' guide at hand, explain the signification of the data in that
 1802 simulation input data file.

1803 (b) Compute and plot a few trajectories and field along, across the sector. Provide
 1804 a graph of field density over the sector.

1805 (c) Compute and plot the radius dependence of the revolution period.

1806 (d) The field indices b_1, b_2, \dots are aimed at realizing the isochronism; four, $b_1 - b_4$
 1807 are accounted for in (a) and (b), they were drawn from the PSI cyclotron spiral sector
 1808 magnet field map data. Question (c) proves this small set of indices to result in a
 1809 poor isochronism of the orbits.

1810 Add higher order indices, until a sufficient number, with proper values, is found
 1811 that allows FIT to reach a final isochronism improved by an order of magnitude.
 1812 Provide a revised input data file with updated index series and their values.

Table 5.2 Simulation input data file: a period of an eight-sector PSI-style cyclotron. The data file is set up for a scan of the periodic orbits, from radius $R=204.1171097$ cm to $R=383.7131468$ cm, in 15 steps

```

PSI CYCLOTRON

'OBJET'
1249.382414
2
1 1
204.1171097 8.915858372 0. 0. 0. 1. 'o'
1
'PARTICUL'
PROTON

'CYCLOTRON'
2
1 45.0 276. 1.0
0. 0. 0.99212277 51.4590015 0.5 800. -0.476376328 2.27602517e-03 -4.8195589e-06 3.94715806e-09
18.3000E+00 1. 28. -2.0
8 1.1024358 3.1291507 -3.14287154 3.0858059 -1.43545 0.24047436 0. 0. 0.
11.0 3.5 35.E-3 0.E-4 3.E-8 0. 0. 0.
18.3000E+00 1. 28. -2.0
8 0.70490173 4.1601305 -4.3309575 3.540416 -1.3472703 0.18261076 0. 0. 0.
-8.5 2. 12.E-3 75.E-6 0. 0. 0. 0.
0. -1
0 0. 0. 0. 0. 0. 0. 0.
0. 0. 0. 0. 0. 0.
2 10.
0.4
2 0. 0. 0. 0.

'FIT2'
2
1 31 0 [-300.,100]
1 35 0 [.1,3.]
2
3.1 1 2 #End 0. 1. 0
3.1 1 3 #End 0. 1. 0
'FAISCEAU'

'FAISTORE'
orbits.fai
1

'REBELOTE'
14 0.2 0 1
1
OBJET 30 221.065356:383.7131468

'SYSTEM'
1
gnuplot <./gnuplot_orbits.gnu
'END'

```

1813 **References**

- 1814 1. J.M. Schippers, J.M.: The Superconducting Cyclotron and Beam Lines of PSI's New
 1815 Proton Therapy Facility "PROSCAN". 17th International Conference on Cyclotrons and their
 1816 Applications: Tokyo, Japan; 18-22 October 2004.
 1817 http://accelconf.web.cern.ch/c04/data/CYC2004_papers/20B2.pdf. Copyrights under license
 1818 CC-BY-3.0, <https://creativecommons.org/licenses/by/3.0/>; no change to the material
- 1819 2. Seidel, M.: Production of a 1.3 Megawatt Proton Beam at PSI. Proceedings of IPAC'10,
 1820 Kyoto, Japan, TUYRA03.
 1821 http://accelconf.web.cern.ch/IPAC10/talks/tuyra03_talk.pdf. Copyrights under license CC-
 1822 BY-3.0, <https://creativecommons.org/licenses/by/3.0/>; no change to the material
- 1823 3. Kawaguchi, T., et al., Design of the sector magnets for the RIKEN superconducting ring
 1824 cyclotron, Proceedings of the 15th International Conference on Cyclotrons and their Applica-
 1825 tions, Caen, France.
 1826 <https://accelconf.web.cern.ch/c98/papers/b-14.pdf>
- 1827 4. <http://accelconf.web.cern.ch/c07/OTHERS/Cyclotron%20List%202007%20-Full.pdf>
- 1828 5. Thomas, L.H.: The Paths of Ions in the Cyclotron. Phys. Rev. 54, 580, (1938)
- 1829 6. Thomas, L.H.: Motion of the spinning electron. Nature. 117 (2945): 514 (1926)
- 1830 7. Symon, K.R., et al.: Fixed-Field Alternating-Gradient Particle Accelerators. Phys. Rev. 103,
 1831 1837 (1956)
- 1832 8. Stambach, T.: Introduction to Cyclotrons. CERN accelerator school, cyclotrons, linacs and
 1833 their applications, IBM International Education Centre, La Hulpe, Belgium, 28 April-5 May
 1834 1994. Copyright/License CERN CC-BY-3.0 - https://creativecommons.org/licenses/by/3.0
- 1835 9. Miller, P.S., et al.: The Magnetic Field of the K500 Cyclotron at MSU Including Trim Coils and
 1836 Extraction Channels. Procs. 9th Int. Conf. on Cyclotrons and their Applications, September
 1837 1981, Caen, France.
 1838 <http://accelconf.web.cern.ch/c81/papers/ep-05.pdf>
- 1839 10. Bethe, H.A. and Rose, M.E., Phys. Rev. 54, 588 (1938)
- 1840 11. After Baartman, Rick: Cyclotrons, Classic to FFAG. FFAG Workshop ***** to be completed
 1841 *****.
- 1842 12. © The Regents of the University of California, Lawrence Berkeley National Laboratory
- 1843 13. Craddock, M.K.: AG focusing in the Thomas cyclotron of 1938, Proceedings of PAC09,
 1844 Vancouver, BC, Canada, FR5REP1.
 1845 <http://accelconf.web.cern.ch/PAC2009/papers/fr5rep113.pdf>
- 1846 14. Joho, W.: The Cyclotron Facilities at PSI. Seminar slides, PSI, 2013 (unpublished)
- 1847 15. Froissart, M., Stora, R.: Depolarisation d'un faisceau de protons polarises dans un synchrotron.
 1848 Nuclear Instruments and Methods. 7 (3): 297-305 (June 1960)
- 1849 16. Méot, F.: Zgoubi Users' Guide.
 1850 <https://www.osti.gov/biblio/1062013-zgoubi-users-guide> Sourceforge latest version:
 1851 <https://sourceforge.net/p/zgoubi/code/HEAD/tree/trunk/guide/Zgoubi.pdf>